Elastic-property measurements of ultrathin films using atomic force acoustic microscopy

M Kopycinska-Müller[1], R H Geiss, J Müller and D C Hurley

Materials Reliability Division, National Institute of Standards and Technology,
325 Broadway, Boulder, CO 80303-3328, USA

E-mail: kopycins@boulder.nist.gov

Abstract

Atomic force acoustic microscopy (AFAM), an emerging technique that
affords nanoscale lateral and depth resolution, was employed to measure the
elastic properties of ultrathin films. We measured the indentation modulus
M of three nickel films approximately 50, 200, and 800 nm thick. In
contrast to conventional methods such as nanoindentation, the AFAM results
remained free of any influence of the silicon substrate, even for the 50 nm
film. X-ray diffraction and scanning electron microscopy results indicated
that the films were nanocrystalline with a strong preferred (111) orientation.
Values of M ranged from 210 to 223 GPa, lower than expected from values
for bulk nickel. The reduced values of the elastic modulus may be attributed
to grain-size effects in the nanocrystalline films.

1. Introduction

Thin films find use in a wide variety of applications, including
microelectromechanical systems (MEMS) and other sensors
and actuators, electronics, and protective and functional
coatings. Knowledge about a film's mechanical properties
allows modelling and prediction of its behaviour under
different conditions. In many cases, the elastic properties of a
thin film vary from those of the corresponding bulk material
because they depend on the conditions of the deposition
process.

As films get thinner, determination of their elastic
properties becomes a challenge due to the complexity of
the film–substrate system. Thus measuring the mechanical
properties of today's thin films requires techniques with a
decreasing interrogation volume. Nanoindentation [1, 2] is
one of the most commonly used methods to determine the
mechanical properties of thin-film samples. However, the
applicability of nanoindentation is severely restricted as the
film thickness decreases. For ultrathin films—those with
thickness less than 1 μm—nanoindentation measurements are
not usually free of the influence of the substrate [3]. Therefore,

the measured elastic properties change with the indentation
depth. It is necessary to explicitly model the properties of
the substrate as well as the film in order to obtain correct
values for the film properties from nanoindentation data [3–
5]. Such models demand careful, tedious characterization
of the indenter and the determination of various instrument-
dependent parameters. Moreover, the volume sampled by
nanoindentation is usually much larger than 10^{-4} μm^3 (the
volume that results from a contact diameter of 100 nm) due to
the relatively large radius and high modulus of the indenter tip
and the relatively large loads applied during the measurement.

In response to this challenge, alternate methods are being
developed. A solution proposed by Asif *et al* [6] involves
a combination of the nanoindentation technique with the
scanning and imaging abilities of atomic force microscopy
(AFM) [7]. The loads applied in this hybrid technique are
lower than in a standard nanoindentation experiment, but the
lateral resolution is still limited by the radius of the Berkovich
diamond indenter (a few hundred nanometres) used. Other
AFM-based techniques capable of high-resolution quantitative
and qualitative characterization of elastic properties involve
dynamic enhancements of the AFM, e.g., ultrasonic force
microscopy, heterodyne force microscopy [8], ultrasonic
atomic force microscopy [9], and atomic force acoustic

---

[1] Author to whom any correspondence should be addressed.
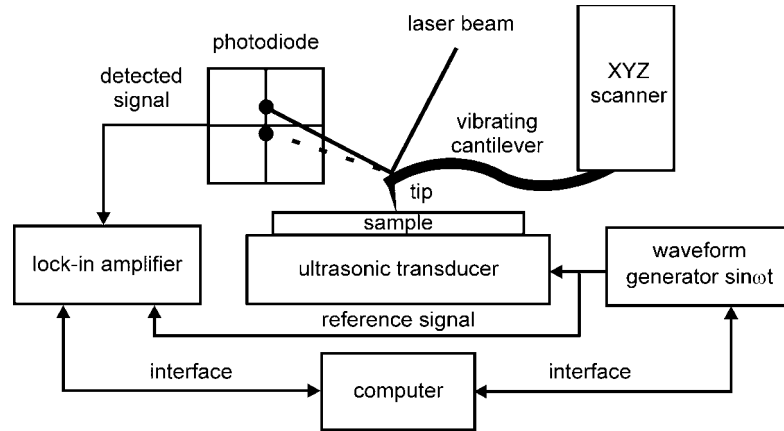
Figure 1. Schematic representation of AFAM apparatus.

microscopy (AFAM) [10, 11]. AFM-based techniques have also been used to investigate the mechanical properties of thin-film samples, e.g. hardness [12]. The influence of film thickness on the tip–sample contact stiffness was evaluated from cantilever vibrations at ultrasonic frequencies [13], and relative elastic properties of thin diamond-like-carbon coatings have been measured with the AFAM technique [14].

In this study, we used the AFAM technique to determine the elastic properties of nickel (Ni) thin-film samples. The elastic modulus of nickel is relatively high (220–250 GPa), but as shown below, even for stiff materials the stress fields created in the AFAM experiment are small enough to probe a small sample volume. This paper is divided into three main parts. The first focuses on the concept of the AFAM technique and the experimental procedure. The second describes the preparation and microstructural characterization of the thin-film samples. The experimental results, their discussion and a theoretical justification of our conclusions are reported in the last part.

2. The AFAM technique

AFAM is a dynamic AFM technique that relies on measuring the resonant frequencies of an AFM cantilever (the 'contact-resonance frequencies') when it is in contact with the sample surface. Quantitative AFAM methods to measure the elastic properties of surfaces and thin films are described in detail elsewhere [11, 14, 15]. We will only summarize the key concepts here. The experimental AFAM apparatus is presented schematically in figure 1. The sample is mounted on an ultrasonic transducer driven by a waveform generator. The transducer emits longitudinal waves, causing out-of-plane surface vibrations in the sample. These vibrations are coupled to the AFM cantilever beam through the tip when it is in contact with the sample surface. Changes in the amplitude of the cantilever vibration are detected by the AFM photodiode sensor using a lock-in amplifier. As the excitation frequency approaches the resonance of the cantilever, the detected amplitude of the cantilever vibrations increases, allowing one to determine the resonance frequency. The amplitude is recorded together with the corresponding ultrasonic frequency to obtain the contact-resonance spectrum. The values of the contact-resonance frequencies are greater than those measured

for the corresponding modes in free space (the 'free-resonance frequencies'). Various tip–sample interaction forces are responsible for the stiffening of the system and the observed shift of the resonance frequencies. In the simplest model, the coupling between the tip and the surface is described by a single spring of constant k^* that represents the tip–sample interaction forces. The static loads applied to the cantilever in AFAM experiments are typically much higher than the adhesion forces, but are still low enough to avoid plastic deformation of the surface. Therefore, elastic forces dominate the tip–sample interaction, and the spring constant k^* that couples the tip and the sample represents the tip–sample contact stiffness. In the AFAM technique, values of k^* are obtained from the measured frequency spectra using a beam-dynamics model that describes the vibrations of the surface-coupled cantilever.

From the AFAM values of k^*, the Hertzian contact-mechanics model [16, 17] can be used to calculate the elastic properties of the probed material. For a hemispherical tip of radius R pressed against a flat surface with force F_C, the resulting contact stiffness k^* can be calculated from

$$k^* = 2a_C E^* = \sqrt[3]{6F_C R E^{*2}}. \tag{1}$$

Here a_C is the contact radius and E^* is the reduced Young's modulus, defined as [18]

$$\frac{1}{E^*} = \frac{1}{M_i} + \frac{1}{M_s}, \tag{2}$$

where M_i and M_s are the indentation modulus of the indenter or AFAM cantilever tip and the sample, respectively. The left equality in equation (1) is true for all geometries while the right equality of the equation can be used only for tips with hemispherical geometry.

The indentation modulus M_s of the sample is calculated from values of k^* using Hertzian or other contact-mechanics models [16]. Such models require information about the contact area or tip geometry, which is usually difficult to determine experimentally. AFAM measurements avoid direct measurement of such tip properties by comparing the value of k^* obtained for the unknown sample to that of a reference sample with known elastic properties:

$$E_s^* = E_{\text{ref}}^* \left(\frac{k_s^*}{k_{\text{ref}}^*} \right)^n. \tag{3}$$
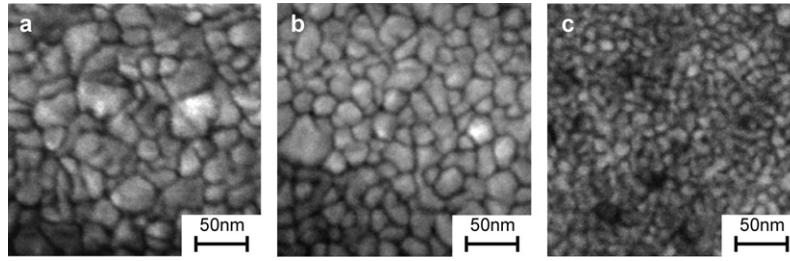
Figure 2. Plan-view SEM images of nickel films with varying thickness t: (a) $t \approx 800$ nm, (b) $t \approx 200$ nm, and (c) $t \approx 50$ nm. Note that the average grain diameter decreases with decreasing t.

Table 1. Properties of nickel thin-film samples. The film thickness t and average grain diameter d were measured from cross-sectional and plan-view SEM images of the samples. The roughness coefficient R_q, which represents the standard deviation in surface height, was calculated from AFM tapping-mode images of the surface of each sample.

Sample no.	t (nm)	d (nm)	R_q (nm)
1	772 ± 5	23 ± 8	1.2
2	204 ± 4	20 ± 6	0.6
3	53 ± 2	11 ± 3	0.5

The subscripts s and ref refer to the unknown and reference sample, respectively. The exponent n depends on the tip–sample geometry. In the case of a spherical tip contacting a flat surface (Hertzian contact), $n = 3/2$; for a tip shaped like a flat punch, $n = 1$. The indentation modulus M_s of the sample can be calculated from equations (2) and (3). Explicit descriptions of the mathematical steps to determine values of k^* and consequently values of M from measured AFAM values of the contact-resonance frequencies are given elsewhere [14, 15, 19].

3. Sample preparation and characterization

3.1. Nickel thin-film samples

Thin films of nickel (Ni) were deposited on single-crystal (100)-oriented silicon wafers by room-temperature DC magnetron sputtering techniques. Three samples with nominal film thicknesses of 800, 200 and 50 nm were prepared. The actual thickness t of each film was determined from scanning electron microscopy (SEM) images of the cross section of each film. Values for t are given in table 1 for each sample. These values represent the mean and standard deviation of eight measurements across a sample length of approximately 4 mm. As shown in table 1, the actual value of t differed by no more than 6% from the nominal value for all three samples. For convenience, the films will be identified below using their nominal thicknesses.

3.2. Microstructural analysis of thin-film samples

The x-ray diffraction (XRD) technique was used to determine whether the thin films possessed a preferred grain orientation. All of the measured XRD spectra showed a strong peak at a 2θ-angle of $44.6°$, corresponding to the (111) orientation of the nickel crystal lattice. SEM examination of the films provided more quantitative information about their microstructure. The

SEM images were acquired using an in-lens detector in order to obtain better image contrast between the grains and grain boundaries. Figure 2 displays SEM images of the top surface of each film. It is important to remember that the grey scale of the SEM images does not correspond to the sample height. The figure shows that the average grain diameter d decreased with decreasing film thickness. In figure 2(a) a few large grains ($d \sim 40$–50 nm) can be observed, but grains approximately 20 nm in diameter dominate. As the film thickness decreases, the grain size and shape become more uniform. In the 200 nm film shown in figure 2(b), the grain diameter ranges from 15 to 25 nm, although a few significantly larger (~ 50 nm) grains can be noticed. The SEM image of the 50 nm film, shown in figure 2(c), reveals regular grains approximately 10 nm in diameter. In the same image, one can also observe small pores (dark regions) approximately 10–20 nm in diameter. In order to estimate the average grain diameter in each sample, commercial software was used. The results of the analysis of the SEM images are presented in table 1. The values of d in table 1 clearly indicate that the nickel films were nanocrystalline.

To investigate the surface roughness of the thin-film samples, AFM tapping mode images were acquired. From these images, values for the roughness coefficient R_q were calculated for each sample. We analysed an area of 2.5×10^5 nm^2, which is much larger than a typical contact area in an AFAM experiment. As can be seen in table 1, the calculated values of R_q are very low—only about 1 nm. Similar values of R_q are usually obtained only for very smooth surfaces such as single-crystal silicon wafers. It can also be noticed that the surface roughness coefficient decreases as the film thickness decreases.

3.3. Reference sample: nickel single crystal

As mentioned above, quantitative AFAM measurements require the use of a reference or calibration sample whose elastic properties are already known. We used a 1.5 mm thick piece of (100)-oriented single-crystal nickel as a reference sample for the experiments described here. Pulse-echo ultrasonic techniques [20] were used to measure the longitudinal and transverse wave velocities V_L and V_T in the $\langle 100 \rangle$ direction of the sample. Assuming the material density $\rho = 8.9 \times 10^3$ kg m^{-3} [21], the second-order elastic moduli c_{11} and c_{44} of the reference sample were determined from the relations $c_{11} = \rho V_L^2$ and $c_{44} = \rho V_T^2$ for wave propagation in the $\langle 100 \rangle$ direction. From the ultrasonic measurements, we obtained $c_{11} = 249.8 \pm 3.3$ GPa and $c_{44} = 118.4 \pm 1.7$ GPa.

These values were nearly identical to the literature values $c_{11} = 250$ GPa, $c_{44} = 118.5$ GPa [21]. We were not able to experimentally determine a value for c_{12}. Taking into account the agreement between our results and the literature values for c_{11} and c_{44}, we assumed the literature value of 160 GPa for c_{12} in the reference sample.

The elastic property obtained in AFAM measurements is the indentation modulus M [10, 19]. For isotropic materials, $M = E/(1 - \nu^2)$, where E is Young's modulus and ν is Poisson's ratio. The calculation of M for an anisotropic material involves various elements of the second-order elastic-constant tensor depending on the direction of indentation [18]. Using the measured values of c_{11} and c_{44}, and the literature value of c_{12}, the value $M_{\langle 100 \rangle} = 219 \pm 2$ GPa for the $\langle 100 \rangle$-oriented nickel sample was calculated. The uncertainty in M is $\pm 1\%$, which is much smaller than the experimental uncertainty in AFAM experiments (typically $\sim 10\%$). To estimate the measurement uncertainty that arises from tip wear and differences between the theoretical and the experimental tip–sample contact geometry, we used the variation in the 17 subsequent AFAM measurements made on the reference sample (see below). A mean value $M = 222 \pm 24$ GPa was obtained, which is within 1% of the expected value $M_{\langle 100 \rangle} = 219$ GPa.

3.4. AFAM measurements

We performed our AFAM experiments using a silicon cantilever with spring constant $k_c = 44$ N m^{-1}, as specified by the vendor. The measured free-space resonance frequencies were respectively 168 and 1042 kHz for the first and the second bending modes. The contact-resonance spectra were measured in the frequency ranges 670–720 kHz (first mode) and 1700–1850 kHz (second mode). Each of the thin-film samples was measured at five different locations. At each position, the contact-resonance frequencies were measured for three different cantilever deflections of 20, 40 and 60 nm. Given the vendor value of $k_c = 44$ N m^{-1}, the deflections corresponded to static loads $F_c = 880$, 1760 and 2640 nN. The tip geometry was characterized using reference measurements performed on the single-crystal nickel sample. Taking into account that k^* increased with the applied static load, we assumed a spherical tip geometry ($n = 3/2$). In each set of experiments a reference measurement was performed both before and after each measurement on a thin-film sample. Such a procedure allowed us to account for tip wear. We calculated values for M for each measurement position by averaging the values obtained at each static deflection. These values will be referred to in the text as 'locally averaged'.

4. Results and discussion

4.1. Experimental results

The locally averaged values of M and the corresponding standard deviations are presented in figure 3. Using values for the elastic constants of single-crystal nickel available in the literature [21], we calculated the range of the expected values of M. Because the $\langle 100 \rangle$ and $\langle 111 \rangle$ directions are the most compliant and stiffest directions of single-crystal nickel, respectively, the corresponding values of $M_{\langle 100 \rangle}$ and $M_{\langle 111 \rangle}$
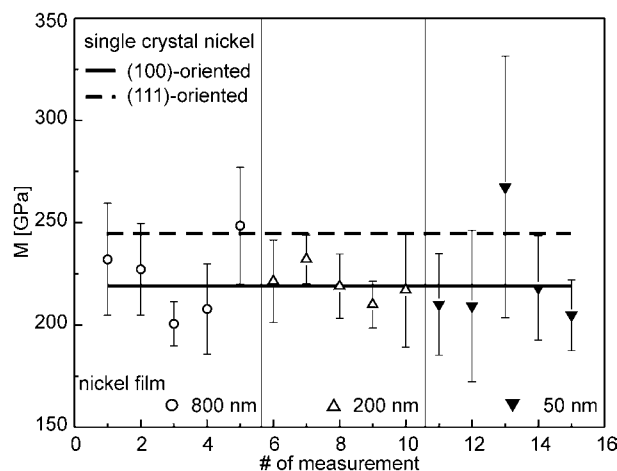

Figure 3. Experimental values of the indentation modulus M of nickel thin films. Also indicated are the values of $M_{\langle 100 \rangle}$ (solid line) and $M_{\langle 111 \rangle}$ (dashed line) calculated from literature values of elastic constants.

Table 2. Values of the indentation modulus M of the nickel thin-film samples. The values M_{AFAM} show the mean and standard deviation for each sample calculated from 30 individual values. The values of the effective indentation modulus M_{eff} were calculated taking into account the volume fraction, lower density, and lower modulus of the intercrystalline phase. The error bars for M_{eff} were calculated using the values of the standard deviation associated with the average grain diameters.

t, nominal (nm)	800	200	50
M_{AFAM} (GPa)	223 ± 28	220 ± 19	210 ± 26
M_{eff} (GPa)	230 ± 7	226 ± 7	208 ± 10

are indicated in figure 3. Considering that our XRD analysis indicated a strongly preferred (111) orientation, one might expect the values of M for the thin-film samples to fall close to $M_{\langle 111 \rangle}$ for single-crystal nickel. However, the measured values of M are closer to $M_{\langle 100 \rangle} = 220$ GPa. The values of M obtained for the 800 and 200 nm films are scattered between 200 and 250 GPa. For the 50 nm film, all but one of the values of M are lower than $M_{\langle 100 \rangle}$ for single-crystal nickel. The remaining (third) measurement stands out due to its high value of $M = 267$ GPa and very large ($\sim 50\%$) error bars. We suspect that during the third measurement, the sample topography in the probed region differed from that of the flat surface assumed in the Hertz model. In this case the measured tip–sample contact stiffness did not increase with the increasing static load, as expected, resulting in widely scattered values of M.

The five locally averaged values of M for each sample were averaged to obtain a single value of M (representing a total of 30 individual values) for each sample. These averages and the corresponding standard deviations are shown in table 2. The averaged values range from 220 to 223 GPa. In the case of the 50 nm sample, we recalculated the average, neglecting the third measurement to obtain $M = 210 \pm 26$ GPa. We repeated AFAM measurements for the 50 nm sample using a different cantilever. The average value of M calculated from 20 measurements was 215 ± 20 GPa. This result is in very good agreement with the recalculated value of M. Although there is a slight decrease in M with decreasing
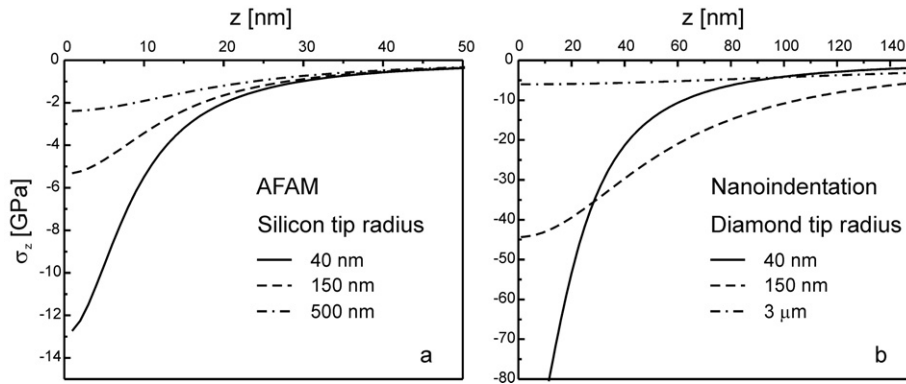
Figure 4. The stress field σ_z in an isotropic sample with $M = 220$ GPa calculated for (a) a spherical silicon indenter used in AFAM experiments and (b) a spherical diamond indenter used in nanoindentation experiments. The different curves were calculated using different values of the tip radius R. Note the difference in scale from (a) to (b) for both horizontal and vertical axes.

film thickness, the numbers are the same within experimental uncertainty. In order to establish whether the decrease is real, further measurements and improved models of the tip–sample contact are needed.

4.2. Thickness effects

According to the calculations in [18], the indentation modulus of a $\langle 111 \rangle$ fibre-textured material with an elastic anisotropy factor greater than 2 is only a few per cent higher than the indentation modulus of the corresponding untextured polycrystalline material. For the nickel films investigated in this study, we therefore expect $M \approx 240$–250 GPa corresponding to $\langle 111 \rangle$-textured nickel. The experimental values of M are 8–12% lower than this. Because the results obtained for all of the samples are very similar, we believe that the observed decrease in stiffness has the same origin. Either it is due to the microstructure of the films, or the films are too thin and the substrate influences the measured values of M. To resolve this issue, we analysed the influence of film thickness on the measured contact stiffness. The results of AFAM or nanoindentation experiments will be free from the influence of the substrate only if the amplitude of the stress field at the film–substrate interface is too small to significantly deform the substrate. In order to estimate the stress present under the indenter, we used the Hertz contact model. The stress σ_z acting along the z-axis into the sample is given by [16]

$$\sigma_z = -p_{\max} \left(1 + \frac{z^2}{a_c^2} \right)^{-1}. \tag{4}$$

Here $p_{\max}$ is the maximum applied pressure, defined in the Hertzian contact model as

$$p_{\max} = \frac{3F_C}{2\pi a_c^2}. \tag{5}$$

Figure 4(a) shows the stress field σ_z created in a simulated AFAM experiment when a silicon tip is pressed against a sample with $M_s = 220$ GPa. For the sake of simplicity, we assumed that the substrate was elastically isotropic. AFM cantilevers typically used in AFAM experiments are made of single-crystal silicon with the tip nominally oriented in the $\langle 100 \rangle$ direction. The indentation modulus $M_{\text{tip}} = M_{\text{Si}\langle 100\rangle} =$

165 GPa was calculated from literature values of the second-order elastic constants of silicon [19]. In AFAM experiments, R can typically range from approximately 20–500 nm. The static load F_c applied in AFAM experiments varies from 20 nN to 2 μN. The curves shown in figure 4(a) were calculated from equations (1), (2) and (5) assuming representative values of the AFM tip radius ($R = 40$, 150, and 500 nm) and a static load of 2 μN. As an approximate comparison to nanoindentation experiments, figure 4(b) shows the corresponding calculations for the stress σ_z created by a spherical diamond indenter pressed against the same material as in figure 4(a). Values of the indenter radius ($R = 40$, 150, and 3 μm) and indentation modulus ($M_{\text{tip}} = M_{\text{diamond}} = 1146$ GPa) representative of commercial tips were used. The maximum indentation load was assumed to be 300 μN. Comparison of figures 4(a) and (b) reveals that the amplitude of the stress field generated by the silicon tip is not only much smaller than that of the diamond indenter, but also decreases more rapidly with depth due to the smaller contact area between the tip and the sample.

As figure 4(a) indicates, the sample volume probed by AFAM is very small—of the order of several hundred to a few thousand cubic nanometres. A commonly accepted rule says that stresses at depths greater than three times the contact radius a_C can be neglected. However, even small stresses present at the film–substrate interface can significantly deform the substrate, depending on the substrate's elastic properties. Consider the following situation. A nickel film is deposited on three substrates with different elastic properties, for instance, a polymeric material, fused quartz, and silicon. The thickness of the films is slightly greater than $3a_C$. The same silicon tip is pressed against each sample at the same static load producing the same stresses at the interface. The resulting deformation of the three substrates at the interfaces is respectively 70%, 7%, and 4% of the deformation at the film surface. These simple estimates show how the substrate can influence the measurement of a thin-film system, even for a film thickness greater than $3a_C$. Therefore, the influence of the substrate on the measurement of the film's elastic properties can be estimated only by a comparison of the deformations occurring at the film surface and film–substrate interface.

Under the specific experimental conditions described here, the estimated surface displacements ranged from 0.7 to 2.5 nm, depending on the tip radius and applied forces. We estimated

the deformation at the interface for these specific AFAM experiments on nickel films. The measured values of the contact stiffness k_{ref}^* were used to back-calculate values for the tip radius R, assuming Hertzian contact mechanics. The values obtained for R varied between 40 and 110 nm. For the samples with films 200 and 800 nm thick, the stress field created by a silicon tip with $R = 40–110$ nm generated a negligible displacement ($\ll 0.01$ nm) at the film–substrate interface. For the film 50 nm thick, the estimated displacement at the interface was approximately 0.1 nm for the maximum applied force. This displacement is only 3–6% of the surface displacement. Therefore, we believe that for all three samples, the measured values of M represent the elastic properties of only the film.

4.3. Nanocrystalline effects

Since our calculations suggest that the silicon substrate did not affect the measurement, we believe that the observed decrease in M is more likely caused by the microstructure of the thin nickel films. Very often, changes in the elastic properties of nanocrystalline materials originate from changes in the material density caused by closed porosity and/or impurities introduced during the deposition process. In addition to high-resolution SEM imaging, we performed transmission electron microscopy (TEM) imaging of the 50 nm sample. No closed pores were visible in either the SEM or TEM images of the samples in cross section. Chemical content analysis of the TEM image also did not show the presence of impurities. Therefore, we do not believe that porosity caused a reduction in density sufficient to reduce the modulus by the observed amount.

Experimental results showing a reduction in the elastic modulus in nanocrystalline materials have been reported previously. In some studies [22–24], the observed reduction was attributed to the presence of porosity as described above. In other studies where high-purity, porosity-free samples were investigated, the observed reduction in Young's modulus was attributed to a high volume fraction of intercrystalline components [25, 26]. The volume fraction of the intercrystalline components (i.e., grain boundaries and triple junctions) increases strongly as the grain diameter decreases below approximately 30 nm [26]. Because the atomic spacing of the intercrystalline components is greater than that of the crystalline component, the corresponding densities and elastic properties can differ significantly. For example, for nanocrystalline iron, the calculated Young's modulus of the intercrystalline component is less than one third that of crystalline iron [27]. The influence of the intercrystalline component on the effective elastic properties of the nanocrystalline material increases as the grain diameter decreases.

As seen in table 1, the average grain diameters in our nickel thin films are indeed less than 30 nm. We used the models described in [26] and [27] to estimate the values of the effective indentation modulus M_{eff} for our thin-film nickel samples. We used the average grain diameters in table 1 to determine the volume fraction of the intercrystalline component in each sample. We assumed that the indentation modulus of the crystalline component was that of a (111)-oriented nickel single crystal (250 GPa) and that the density

of the intercrystalline phase was 80% of the density of the crystalline phase [28]. The values of M_{eff} obtained from these calculations are shown in table 2. The differences between M_{eff} and the measured values M_{AFAM} are smaller than the measurement uncertainty. Therefore, the results of these simple calculations suggest that grain-boundary effects are the most likely cause of the observed reduction in modulus for the nanocrystalline nickel films.

These results show that AFAM offers a more direct way to measure the elastic properties of very thin (<1 μm) films than nanoindentation. Although both methods determine the same quantity, the indentation modulus M, the critical size and force scales in AFAM experiments are much smaller. As a result, the stress field generated in a sample under typical AFAM conditions is smaller and falls off much more rapidly with distance than the corresponding field for nanoindentation. The two techniques can yield similar results as long as they are applied to a single-crystal sample or to a coarse polycrystalline or composite sample. However, for a system involving a thin film, the amplitude of the stress σ_z ($z = d$) at the film–substrate interface determines whether the tip–sample contact stiffness is free from the substrate influence. The deformation of the film–substrate interface will depend on the film thickness and on the relative elastic properties of the substrate and the film. If the substrate is much stiffer than the film, the situation is relatively straightforward: σ_z generated in the relatively compliant film is low and does not cause significant deformation at the interface. For a very stiff film on a compliant substrate, σ_z can be very large and can even plastically deform the substrate. The samples investigated in this study consisted of a stiffer film on a slightly more compliant substrate, but the relative difference in stiffness was not very large ($M_{\text{Ni}} = 220–250$ GPa, $M_{\text{Si}} = 165$ GPa). In addition, the stresses applied in these experiments were relatively low and insignificantly deformed the substrate. It is important to note that this discussion is valid only if (1) the ratio of film thickness to contact radius $d/a_{\text{c}} > 1$, and (2) the sample deformation remains elastic.

5. Summary and conclusions

We have investigated a series of thin films in order to examine the effect of thickness on elastic-property measurements with AFAM. SEM images showed that the sputtered nickel films were nanocrystalline, with approximate grain sizes from 11 to 23 nm. XRD indicated a strong preferential (111) grain orientation. Values of the indentation modulus M obtained by AFAM were lower than expected from literature values for single-crystal nickel. The decrease in stiffness was observed even for a film 800 nm thick, for which substrate effects are negligible. Analysis indicated that the observed reduction in modulus for all three films could be explained by an increased amount of intercrystalline components in the nanocrystalline films. The calculated stress amplitude at the interface of the 800 nm film was less than 0.03% of the stress present directly under the tip. Calculations of the substrate deformation at the film–substrate interface yielded values less than 1 pm. For the thinnest film that was $\sim$50 nm thick, the estimated amplitude of the stress field at the interface ranged from 3 to 6% of its value under the tip, depending on the assumed tip radius. Such stress deformed the substrate by less than 0.1 nm at the

film–substrate interface. Taking into account the similarity of the measured values for the three samples, we conclude that with AFAM methods it is possible to measure the elastic properties of ultrathin films without taking the properties of the substrate into account. The minimum film thickness for which substrate effects need not be included depends on the geometry and elastic properties of the tip and the elastic properties and roughness of the film–substrate system.

Acknowledgments

References

[1] Oliver W C and Pharr G M 1992 *J. Mater. Res.* **7** 1564
[2] Pharr G M, Oliver W C and Brotzen F R 1992 *J. Mater. Res.* **7** 613
[3] Saha R and Nix W D 2002 *Acta Mater.* **50** 23
[4] King R B 1987 *Int. J. Solids Struct.* **23** 1657
[5] Tang K C and Arnell R D 1999 *Thin Solid Films* **355/356** 263
[6] Syed Asif S A, Wahl K J, Colton R J and Warren O L 2001 *J. Appl. Phys.* **90** 1192
[7] Maivald P, Butt H J, Gould S A C, Prater C B, Drake B, Gurley J A, Elings V B and Hansma P K 1991 *Nanotechnology* **2** 103
[8] Cuberes M T, Assender H E, Briggs G A D and Kolosov O V 2000 *J. Phys. D: Appl. Phys.* **33** 2347
[9] Yamanaka K, Maruyama Y, Tsuji T and Nakamoto K 2001 *Appl. Phys. Lett.* **78** 1939
[10] Rabe U, Kopycinska M, Hirsekorn S, Munoz Saldana J, Schneider G A and Arnold W 2002 *J. Phys. D: Appl. Phys.* **35** 2621
[11] Hurley D C, Shen K, Jennett N M and Turner J A 2003 *J. Appl. Phys.* **94** 2347
[12] Persh G, Born Ch and Utesch B 1994 *Appl. Phys.* A **59** 29
[13] Crozier K B, Yaralioglu G G, Degertekin F L, Adams J D, Minne S C and Quate C F 2000 *Appl. Phys. Lett.* **76** 1950
[14] Amelio S, Goldade A V, Rabe U, Scherer V, Bhushan B and Arnold W 2001 *Thin Solid Films* **392** 75
[15] Rabe U, Amelio S, Kester E, Scherer V, Hirsekorn S and Arnold W 2000 *Ultrasonics* **38** 430
[16] Johnson K L 1985 *Contact Mechanics* (Cambridge: Cambridge University Press)
[17] Sthal F and Cretin B 1995 *Acoustical Imaging* vol 21, ed J P Jones (New York: Plenum)
[18] Vlassak J J and Nix W D 1993 *Phil. Mag.* A **67** 1045
[19] Rabe U, Amelio S, Kopycinska M, Hirsekorn S, Kempf M, Göcken M and Arnold W 2002 *Surf. Interface Anal.* **33** 65
[20] Papadakis E P 1990 *Physical Acoustics* vol 19, ed R N Thurston and A D Pierce (San Diego, CA: Academic)
[21] Simmons G and Wang H 1971 *Single Crystal Elastic Constants and Calculated Aggregate Properties: A Handbook* (Cambridge, MA: MIT Press)
[22] Fougere G E, Riester L, Ferber M, Weertman J R and Siegel R W 1995 *Mater. Sci. Eng.* A **204** 1
[23] Hoffmann M and Birringer R 1996 *Acta Mater.* **7** 2729
[24] Sanders P G, Youngdahl C J and Weertman J R 1997 *Mater. Sci. Eng.* A **234–236** 77
[25] Weller M, Diehl J and Schaefer H-E 1991 *Phil. Mag.* A **63** 527
[26] Zhou Y, Erb U, Aust K T and Palumbo G 2003 *Scr. Mater.* **48** 825
[27] Wang G-F, Feng X-Q, Yu S-W and Nan C-W 2003 *Mater. Sci. Eng.* A **363** 1
[28] Fitzsimmons M R, Röll A, Burkel E, Sickafus K E, Nastasi M A, Smith G S and Pynn R 1995 *Nanostruct. Mater.* **6** 539